Intelligent Analysis of EEG Data for Attention Concentration and Mind Wandering Classification

Vladimir Romaniuk, Alexey Kashevnik
SPC RAS
St. Petersburg, Russian Federation
romanyuk.v@iias.spb.su, alexey.kashevnik@iias.spb.su

***Abstract*—The aim of this study is to evaluate electroencephalographic-based classification of mind wandering, internally directed concentration, and externally directed attention. Data from 32 participants were analyzed using 22 EEG features describing spectral power, the aperiodic spectral component, time-series irregularity, and functional connectivity. Classification was evaluated using single 60-s epochs and recording-level representations based on feature means and temporal summaries. For MINDWANDERING–INTERNAL recording-level analysis reached a macro-F1 of 0.665 after matching the experiment duration, compared with 0.532 for the epoch description and 0.462 for the EEG-feature only representation. Contrasts involving EXTERNAL were more readily separable, with epoch macro-F1 near 0.76 and full-recording macro-F1 of 0.83–0.88, although EXTERNAL also differed in eye state, visual stimulation, and behavioral response. The results indicate that temporal summaries across several minutes provide useful information for distinguishing the two closed-eye instructed conditions that is not captured by individual epochs or mean feature values alone.**

***Index Terms*—electroencephalography, mind wandering, attention, machine learning, cognitive-state classification**

I. Introduction

Human mental activity may differ considerably in the direction and stability of attention. Thoughts may change freely around one topic or without a fixed topic, whereas in another state a person intentionally maintains concentration on a selected object or task. The ability to sustain attention voluntarily can be developed through special practices, including meditation. Objective differentiation of attention states nevertheless remains a separate problem because ongoing mental activity cannot be observed directly and is largely determined from a person's subjective report.

Electroencephalography provides a means of studying changes in brain activity associated with concentration and mind wandering. However, no universal EEG measure has been established that unambiguously separates these states. A systematic review of mind-wandering studies demonstrates that spectral effects vary with the experimental paradigm [1]. Studies of meditative concentration also report changes in spectral, connectivity, and complexity characteristics of EEG, but the results depend on the practice type, participant experience, and analytical method [2].

It is therefore appropriate to formulate attention-state recognition as the analysis of a set of EEG characteristics. In addition to conventional spectral-power measures, nonlinear signal characteristics may contain information about the current state. Differences between mind wandering and concentration have been reported for fractal dimension, Lempel–Ziv complexity, and entropy measures [3]–[6]. Further information may be provided by the aperiodic spectral component and functional-connectivity measures [7]–[9].

TABLE I. Characteristics of the study sample

Group	Participants	Recordings	Age, mean ± SD	F/M
Control	15	22	38.5 ± 10.1	10/5
Yoga practitioners	17	25	35.1 ± 17.4	10/7

A multivariate feature representation makes it possible to move from the search for one physiological marker to the recognition of combinations of characteristics associated with different states. EEG-based classification of mind wandering has been demonstrated both within individual participants and when transferring models between participants [10], including the use of neural-network methods [11], [12]. The possibility of differentiating mind wandering from intentional meditative concentration in the absence of an active external task has been studied to a substantially lesser extent.

The aim of the present study is to evaluate the quality of classifying mind wandering, internally directed concentration, and externally directed attention from a set of EEG features in yoga practitioners and control-group participants.

II. Method for Attention-State Classification

The proposed method consists of identifying the intervals corresponding to the attention states, preprocessing and segmenting the EEG signal, calculating spectral, aperiodic, nonlinear, and connectivity characteristics, forming recording-level and epoch-level representations, and training machine-learning models (Fig. 1).

A. EEG Data

The analysis included data from 32 participants. The control group comprised 15 participants with 22 available recordings. The experimental group comprised 17 yoga practitioners with 25 recordings [13]. The characteristics of the sample are presented in Table I.

EEG was recorded using the ANT Neuro eego mylab system. A 64-channel electrode montage corresponding to the

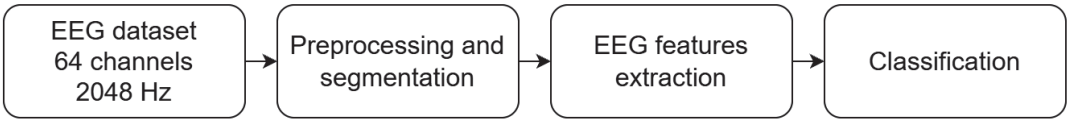


Fig. 1. General scheme of the method for attention-state classification from EEG.

extended international 10–10 system was used. The original sampling frequency was 2048 Hz.

The experimental procedure comprised five consecutive blocks. At the beginning and end of the study, resting-state blocks were recorded with alternating eyes-open and eyes-closed intervals. Between these blocks, the participants performed mind wandering, internal concentration (meditation), and externally directed visual search. During visual search, participants had to find an image fragment on the screen. The protocol is summarized in Table II.

The principal classification analysis included MINDWANDERING, INTERNAL, and EXTERNAL.

B. Preprocessing and Segmentation

A high-pass filter with a cutoff frequency of 1 Hz and a notch filter at 50 Hz were applied to the continuous EEG signal. Electrooculogram and electrocardiogram channels, as well as the M1 and M2 electrodes, were excluded from feature calculation. The analysis did not re-reference the signal or correct artifacts using independent component analysis. The remaining EEG channels were used in the subsequent steps.

The continuous recordings were divided into non-overlapping 60-s intervals. The first and last minutes of each experimental state were excluded from the final aggregation of the measures to reduce the influence of transition processes between states. Networks trained on raw EEG received the multichannel signal after the sampling rate had been reduced to 128 Hz.

C. EEG Features

The feature set contained 22 measures describing spectral power, the aperiodic spectral component, time-series irregularity, and functional connectivity (Table III). The measures were selected on the basis of earlier EEG studies of mind wandering, concentration, complexity, and attention [1]–[9].

Spectral power was estimated using Welch's method with 2-s windows and 50% overlap [14]:

$$\widehat{S}_c(f) = \frac{1}{L}\sum_{\ell=1}^{L} I_{\ell,c}(f), \tag{1}$$

where $I_{\ell,c}(f)$ is the periodogram of window ℓ on channel c, and L is the number of windows. Band power over an interval $B = [f_1, f_2]$ was

$$P_{c,B} = \int_{f_1}^{f_2} \widehat{S}_c(f)\,\mathrm{d}f. \tag{2}$$

The following frequency bands were considered:

- delta, 1–4 Hz;
- theta, 4–8 Hz;
- alpha, 8–13 Hz;
- beta, 13–30 Hz;
- gamma, 30–45 Hz;
- high-frequency gamma, 60–110 Hz.

Relative power used the total power in the 1–40 Hz range as the denominator. Frontal-midline theta activity was defined using electrodes Fz, FCz, and Cz, whereas posterior alpha activity was defined using Pz, Oz, O1, and O2. Individual alpha frequency was defined as the frequency of maximum spectral power in the 7–14-Hz range.

The aperiodic spectral slope was estimated by linear regression in log–log coordinates over the 2–40 Hz range.

$$\log_{10} S_c(f) = a_c \log_{10} f + b_c, \tag{3}$$

where a_c is the aperiodic slope. The corresponding aperiodic spectrum and residual oscillatory component were

$$\widehat{S}_{c,\mathrm{aper}}(f) = 10^{a_c \log_{10} f + b_c}, \tag{4}$$

$$r_c(f) = \max\bigl(S_c(f) - \widehat{S}_{c,\mathrm{aper}}(f), 0\bigr). \tag{5}$$

Residual oscillatory measures for the theta, alpha, beta, and gamma bands were obtained by integrating (5) over the corresponding intervals.

Higuchi fractal dimension D_H was the slope [15]

$$\ln L(k) = D_H \ln(1/k) + b, \qquad k = 1, \ldots, 8, \tag{6}$$

where $L(k)$ is the mean curve length at scale k. Spectral entropy on the 1–40-Hz range was

$$H_{\mathrm{spec}} = -\frac{\sum_{i=1}^{M} p_i \ln p_i}{\ln M}, \qquad p_i = \frac{S(f_i)}{\sum_{j=1}^{M} S(f_j)}, \tag{7}$$

where M is the number of frequency bins. For Lempel–Ziv complexity, the signal x was transformed into a binary sequence relative to its median [16]. After counting the number C of previously unseen substrings,

$$\mathrm{LZC} = \frac{C \log_2 n}{n}, \tag{8}$$

where n is the length of the binary sequence.

Functional connectivity was assessed using an amplitude-weighted imaginary-part index computed from Hilbert analytic

TABLE II. SEQUENCE OF EXPERIMENTAL BLOCKS

Block	Duration	Eye State	Content
REST1	8 min	Alternating	Sequence of intervals with eyes open and closed.
MINDWANDERING	10 min	Closed	Mind wandering.
INTERNAL	15 min	Closed	Internally directed concentration.
EXTERNAL	10 min	Open	Visual-search task.
REST2	8 min	Alternating	Repeated sequence of intervals with eyes open and closed.

signals after band-pass filtering. For channels u and v in band B,

$$C_{uv}^{B} = \frac{\mathrm{E}\left[\left|\mathrm{Im}\left(h_{u,B}(t)\overline{h_{v,B}(t)}\right)\right|\right]}{\mathrm{E}\left[\left|h_{u,B}(t)\overline{h_{v,B}(t)}\right|\right]}, \tag{9}$$

where $h_{u,B}(t)$ and $h_{v,B}(t)$ are the analytic signals. The imaginary part is used to reduce the contribution of zero-lag volume conduction [17].

Theta–alpha connectivity was calculated as the mean of (9) over the pairs Fz–Pz and Fz–Cz and over the theta and alpha bands. Gamma-band connectivity used the same channel pairs and the mean over the gamma and high-gamma bands.

For each of the 22 features, four summaries were calculated within each instructed block:

1) the mean value;
2) the coefficient of the linear temporal trend, defined as the slope of the regression of the value on the epoch number;
3) the mean directed change between consecutive intervals;
4) the mean absolute change between consecutive intervals.

Additional characteristics of the epoch sequence within each condition were calculated: first-order autocorrelation, coefficient of variation, skewness, kurtosis, median, interquartile range, slope between the first and last epochs, and range-to-mean ratio.

Catch22, a fixed set of 22 statistics describing the shape of a time series [18], was calculated for the minute-by-minute sequence of each EEG feature and added to the mean level and measures of within-block change.

D. Classification

Every feature was standardized using the training mean and standard deviation. The same parameters were applied to the test data. The neural models were optimized with AdamW using a learning rate of 10^{-3}, a batch size of 16, and up to 120 epochs. Class-weighted cross-entropy was used to reduce the influence of class imbalance. Training stopped after 20 epochs without improvement on validation set.

Each observation corresponded to one session in one instructed block. Every session from one person remained in one of the training, validation, or test sets. Twenty repeated splits divided the 32 participants among these three sets in a 60/20/20 ratio, corresponding to 20, 6, and 6 participants.

Each session was represented in four ways.

The full recording contained the 22 EEG features and all within-block summaries defined above. The vector had 664 columns and was used to test separation when both EEG level and within-block change were available.

The epoch description contained only the 22 features of a single non-overlapping 60-s interval and no recording summary. It was used to test whether the same separation was present within one minute.

The EEG-feature only representation contained the 22 mean values and omitted the trend, successive changes and sequence statistics.

The matched recordings were used to test whether the full-recording score depended on the unequal lengths of the blocks. The temporal summaries were calculated on blocks that usually contained 8 minutes of mind wandering and 13 minutes of internal concentration, so a full-recording score may reflect the extra minutes rather than a difference between the states. For each session, three windows were cut from internal concentration. Each window was a continuous sequence containing the same number of minutes as the mind-wandering block of that session: the earliest, middle, or latest minutes. The same summaries as in the full recording were then recalculated within each window, which removes this length difference.

Sequence models did not receive these fixed vectors. Instead, they received the feature sequence across the epochs.

The three blocks were compared in the following pairs. MINDWANDERING–INTERNAL was the main pair because both blocks were recorded with closed eyes and without an external task. Each of the other two pairs included the block performed with open eyes, a visual stimulus, and a search response. A three-class task used all three blocks together and tested whether a separation found in a pair remained when all three conditions had to be distinguished simultaneously. The pairs were:

1) MINDWANDERING–INTERNAL;
2) MINDWANDERING–EXTERNAL;
3) INTERNAL–EXTERNAL.

The evaluated models are listed in Table IV. They include linear classifiers, neural ensembles, a fully connected network, spatial filtering, random convolutional kernels, and compact convolutional networks for EEG. All models were implemented using PyTorch.

The linear family used a single fully connected layer from the input dimension to two class logits. The L_2-regularized linear classifier was trained with class-weighted cross-entropy and weight decay of 10^{-3}.

The multilayer perceptron contained one hidden layer of 32 units for binary tasks. Each hidden layer comprised an affine

TABLE III. THE 22 EEG FEATURES USED IN CLASSIFICATION

Feature	Class	Formula
Absolute alpha power	Spectral	P_α in (2), $B = [8, 13]$ Hz
Relative alpha power	Spectral	$P_\alpha / P_{[1,40]}$
Theta power	Spectral	P_θ in (2), $B = [4, 8]$ Hz
Beta power	Spectral	P_β in (2), $B = [13, 30]$ Hz
High-frequency gamma power	Spectral	$P_{\mathrm{h}\gamma}$ in (2), $B = [60, 110]$ Hz
Alpha-to-theta ratio	Spectral	P_α / P_θ
Theta-to-alpha ratio	Spectral	P_θ / P_α
High-gamma to theta–alpha ratio	Spectral	$P_{\mathrm{h}\gamma} / (P_\theta + P_\alpha)$
Frontal-midline theta	Spectral	P_θ at Fz, FCz, Cz
Posterior alpha power	Spectral	P_α at Pz, Oz, O1, O2
Individual alpha frequency	Spectral	$\arg\max_{f \in [7,14]} \widehat{S}(f)$ from (1)
Posterior individual alpha frequency	Spectral	same, at Pz, Oz, O1, O2
Aperiodic slope	Aperiodic	a in (3)
Residual oscillatory theta	Aperiodic	$\int_4^8 r(f)\,\mathrm{d}f$ from (5)
Residual oscillatory alpha	Aperiodic	$\int_8^{13} r(f)\,\mathrm{d}f$ from (5)
Residual oscillatory beta	Aperiodic	$\int_{13}^{30} r(f)\,\mathrm{d}f$ from (5)
Residual oscillatory gamma	Aperiodic	$\int_{30}^{45} r(f)\,\mathrm{d}f$ from (5)
Higuchi fractal dimension	Complexity	D_H in (6)
Spectral entropy	Complexity	H_{spec} in (7)
Lempel–Ziv complexity	Complexity	LZC in (8)
Theta–alpha connectivity	Connectivity	C_{uv}^B in (9), $B \in \{\theta, \alpha\}$
Gamma-band connectivity	Connectivity	C_{uv}^B in (9), $B \in \{\gamma, \mathrm{h}\gamma\}$

TABLE IV. MODELS INCLUDED IN THE MACHINE-LEARNING COMPARISON

Implemented model	Input representation
L_2-regularized linear classifier	Vector of calculated features
Linear hinge classifier	Vector of calculated features
Bagged neural ensemble	Vector of calculated features
Additive residual neural ensemble	Vector of calculated features
Multilayer perceptron	Vector of calculated features
CSP + linear classifier	Spatially filtered feature sequences
Random convolutional kernel transform	Sequence of features across epochs
EEGNet-lite	Decimated multichannel EEG
Shallow convolutional network	Decimated multichannel EEG

transformation, layer normalization, a GELU nonlinearity, and dropout with probability 0.25. The output layer produced class logits. This architecture provided a compact nonlinear baseline on the same standardized feature vectors as the linear models.

The bagged neural ensemble averaged 100 two-layer modules with a hidden width of 12 units and a ReLU activation. Each learner received all input features. An additional bagged variant used random feature masks that retained 70% of the variables. The additive residual neural ensemble summed 40 such modules with a stage weight of 0.1.

The random convolutional kernel transform received an aligned sequence of epoch-level feature vectors. Sixty-four random one-dimensional convolutional kernels of length 9 were applied across the feature channels. For each kernel, the maximum of the convolution and the maximum of its negation were retained, which produced a 128-dimensional representation. A linear layer mapped this representation to class logits.

The CSP + linear classifier estimated common spatial patterns from the two-class covariance matrices of the multichannel series. Four spatial filters were formed from the extreme generalized eigenvectors. Each trial was reduced to a four-dimensional vector of log-variance of the spatially filtered series. A linear layer mapped this vector to class logits and was trained with class-weighted cross-entropy. When a contrast contained fewer than two training observations in one class, the spatial filters were replaced by a channel-wise temporal mean followed by the same linear layer.

EEGNet-lite followed the scheme of Lawhern *et al.* [19]. The first block applied eight temporal convolutions of length 64, followed by a depthwise spatial convolution over the EEG channels, batch normalization, an ELU nonlinearity, average pooling with a factor of four, and dropout 0.25. The second block applied a depthwise separable temporal convolution of length 16, batch normalization, ELU, average pooling with a factor of eight, and dropout 0.25. Adaptive average pooling and a linear layer produced the class logits.

The shallow convolutional network used 16 temporal filters of length 25, followed by a depthwise spatial convolution that expanded the representation to 32 feature maps, batch normalization, ELU, average pooling with a factor of eight,

and dropout 0.5 before adaptive pooling and a linear classifier.

CSP, EEGNet-lite, and the shallow network read the EEG signal rather than the 664-column vector.

E. Evaluation

The primary reporting metric was the F1-score. For class k,

$$\mathrm{F1}_k = \frac{2\,\mathrm{Precision}_k\,\mathrm{Recall}_k}{\mathrm{Precision}_k + \mathrm{Recall}_k}, \tag{10}$$

and the reported value was the macro-average

$$\mathrm{F1} = \frac{1}{K}\sum_{k=1}^{K}\mathrm{F1}_k, \tag{11}$$

where K is the number of classes. All reported scores are macro-F1, which assigns equal weight to each class.

Validation participants were excluded from training and from the final test. The reported model for each contrast is the one with the highest mean macro-F1 on validation set. The reported value is the mean of the 20 test scores. The $\pm$ term is the standard deviation of the 20 test scores and describes variability across participant splits.

III. Classification Results

Fig. 2 compares the evaluated models on the full recording. Table V gives, for each contrast, the test score of the best model on three descriptions: one 60-s epoch, the full recording, and the matched recording. The best model is the one selected by the highest mean macro-F1 on the validation set.

On the full recording, MINDWANDERING–INTERNAL reached 0.851 ± 0.043 with the bagged ensemble, MINDWANDERING–EXTERNAL reached 0.833 ± 0.048 with the additive residual ensemble, and INTERNAL–EXTERNAL reached 0.876 ± 0.044 with the bagged ensemble. On the matched recording, MINDWANDERING–INTERNAL reached 0.665 ± 0.052 with the bagged ensemble. All three instructed-condition pairs therefore showed above-chance classification performance when the full-recording representation was used.

The Epoch columns of Table V are epoch-level classification: each observation is one 60-s interval, described only by its 22 features. MINDWANDERING–INTERNAL reaches 0.532 ± 0.024 with the multilayer perceptron, so this description does not support continuous monitoring of the two closed-eye conditions. MINDWANDERING–EXTERNAL reaches 0.755 ± 0.036 with the additive residual ensemble, and INTERNAL–EXTERNAL reaches 0.767 ± 0.047 with the bagged ensemble.

Fig. 3 shows corresponding differences in relative alpha power, posterior alpha power, and Lempel–Ziv complexity as an example of the differences between the three conditions. EXTERNAL distributions differ from the two closed-eye conditions, whereas MINDWANDERING and INTERNAL overlap.

A. Three-Class Classification

All evaluated models were also tested when MINDWANDERING, INTERNAL, and EXTERNAL had to be distinguished together (Fig. 4). The figure shows the test score of the best model for each representation. The best model is the one selected by the highest mean macro-F1 on the validation set. On the full recording, the additive residual ensemble reached 0.768 ± 0.045. On the matched recording, the middle INTERNAL window, the bagged ensemble reached 0.572 ± 0.055. At epoch level, linear discriminant analysis (LDA) reached 0.474 ± 0.035. Each confusion matrix sums the predictions across the 20 participant splits.

B. Effect of Recording Duration

The matched recording compares the unequal full recording with INTERNAL windows of the same length as mind wandering.

For MINDWANDERING–INTERNAL, the bagged ensemble with 70% feature masks scores 0.850 ± 0.054 on the unequal full recording and 0.576 ± 0.049, 0.665 ± 0.052, and 0.622 ± 0.057 on the earliest, middle, and latest equal-length windows (Table VI, Fig. 5). A large part of its full-recording score does not remain when the sequences have the same length.

For INTERNAL–EXTERNAL, the bagged ensemble scores 0.832 ± 0.041 on the earliest window. This pair was already separable in one minute, and the reduction is smaller than for the closed-eye pair.

C. Feature Importance

This analysis estimates which feature families account for classification of MINDWANDERING–INTERNAL. In the full recording, catch22 is included together with the mean, the trend, and the successive changes. For the comparison in Fig. 6, the bagged ensemble was trained on the columns of one family at a time, on the unequal full recording and on the middle-minute window.

On the matched middle window, the EEG-feature only representation containing only the 22 mean values reached a macro-F1 of 0.462, whereas the full temporal representation reached 0.665 ± 0.052.

Catch22 columns, entered without the trend and successive-change columns, gave the highest score in this comparison – 0.820 ± 0.052 on the unequal full recording and 0.616 ± 0.049 on the middle minutes.

Trend and successive changes, excluding the catch22 columns, scored 0.638 ± 0.063 on the full recording and 0.610 ± 0.079 on the middle minutes.

Families that describe the signal level remained at or below 0.5 on both recordings. These were the spectral means, complexity, including spectral entropy, the aperiodic slope, and connectivity.

IV. Discussion

A. Discrimination of Internal States

For MINDWANDERING–INTERNAL, matching the recording duration substantially reduced classification

TABLE V. TEST SCORE OF THE BEST MODELS ON THE EPOCH, THE FULL RECORDING, AND THE MATCHED RECORDING

Contrast	Epoch model	Epoch	Full-recording model	Full recording	Matched-recording model	Matched recording
MINDWANDERING–INTERNAL	Multilayer perceptron	0.532 ± 0.024	Bagged ensemble	0.851 ± 0.043	Bagged ensemble	0.665 ± 0.052
MINDWANDERING–EXTERNAL	Additive residual	0.755 ± 0.036	Additive residual	0.833 ± 0.048	Additive residual	0.833 ± 0.048
INTERNAL–EXTERNAL	Bagged ensemble	0.767 ± 0.047	Bagged ensemble	0.876 ± 0.044	Bagged ensemble	0.710 ± 0.054

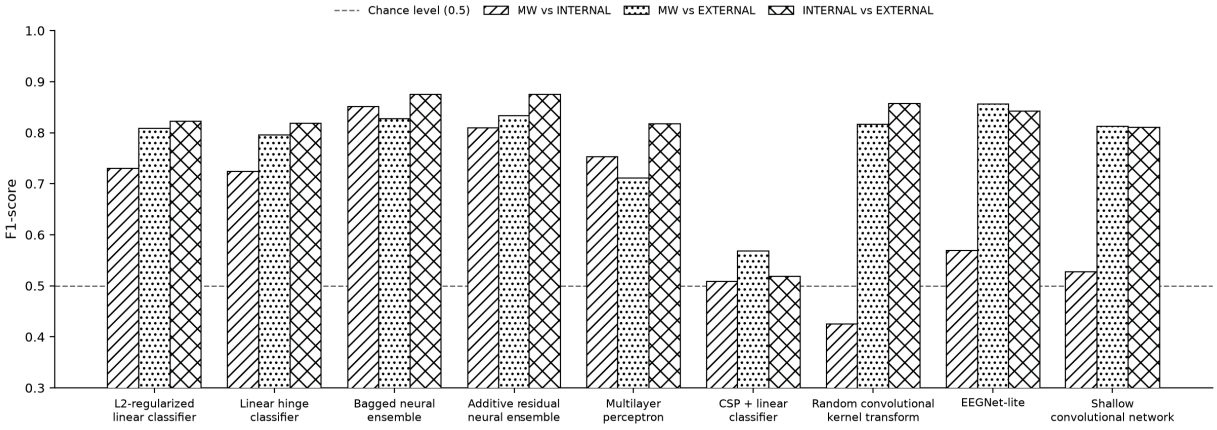


Fig. 2. Test macro-F1 of the evaluated models.

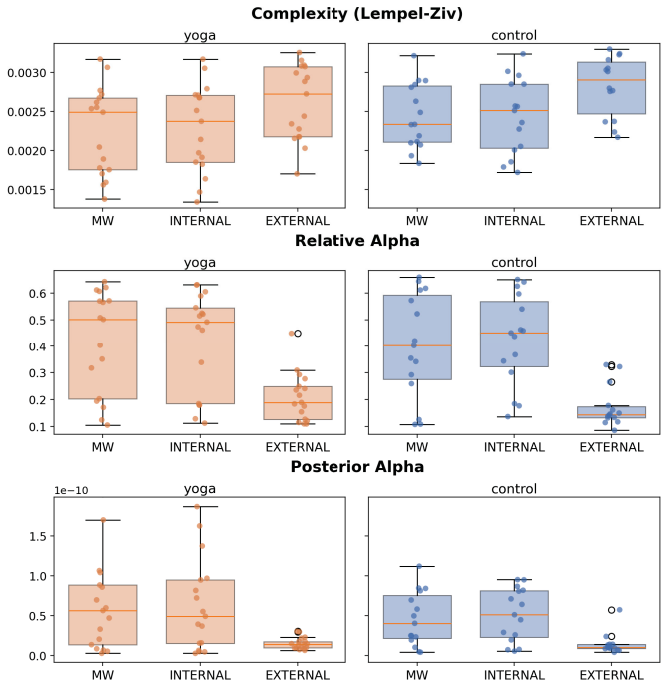


Fig. 3. Relative alpha power, posterior alpha power, and Lempel–Ziv complexity by condition.

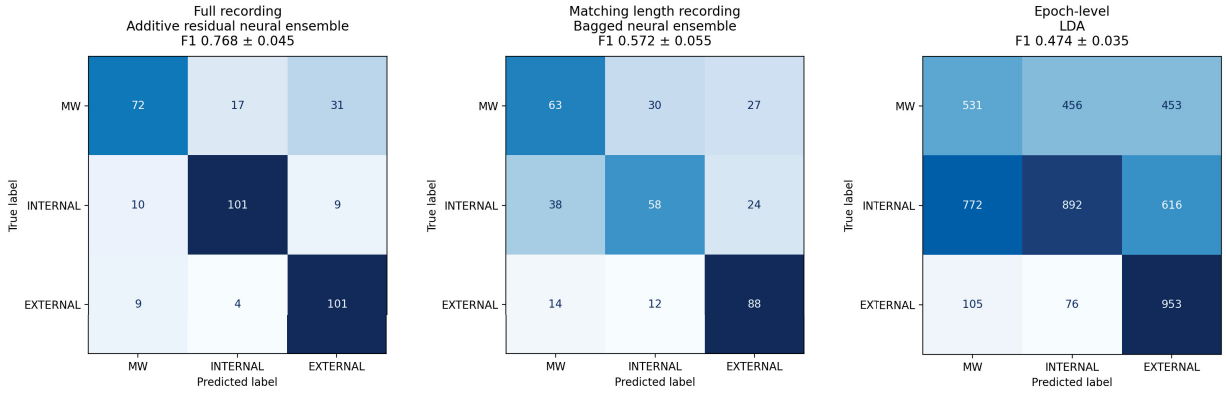


Fig. 4. Aggregated three-class confusion matrices for the best model on each representation

TABLE VI. MINDWANDERING–INTERNAL MACRO-F1 ON THE FULL RECORDING AND ON EQUAL-LENGTH WINDOWS.

INTERNAL window	Macro-F1
Full recording, unequal length	0.850 ± 0.054
Earliest minutes	0.576 ± 0.049
Middle minutes	0.665 ± 0.052
Latest minutes	0.622 ± 0.057

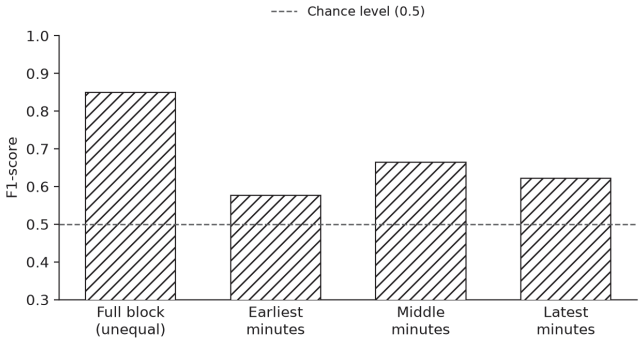


Fig. 5. MINDWANDERING–INTERNAL macro-F1 for the full recording and equal-length INTERNAL windows.

performance compared with the unequal full recording. This suggests that the strong separation observed on the full recording was partly related to the difference in sequence length, while a more moderate distinction between the two closed-eye conditions remained after this factor was removed.

B. Role of Temporal Summaries

The feature-family analysis showed that catch22, trend, and successive changes were more informative than feature families describing the signal level. This suggests that changes in EEG-derived features during the instructed block contribute more to the separation of MINDWANDERING and INTERNAL than stable differences in their average values. The differences between the earliest, middle, and latest INTERNAL windows also indicate that the separation is not uniform throughout the block. In particular, the lower score for the earliest minutes may reflect the transition from the preceding MINDWANDERING block, although this cannot be established from the present experimental design.

C. Role of the External Visual Task

The contrasts involving EXTERNAL were easier to classify, including at the epoch level. However, EXTERNAL differed from the two internal conditions not only in attention direction, but also in eye state, visual stimulation, and behavioral response. The observed separation therefore reflects differences between the experimental conditions as a whole rather than isolated recognition of externally directed attention.

D. Experimental Design and Generalizability

The analysis was based on 32 participants. Although repeated participant-level splits and standard deviations across splits were used, validation on an independent dataset is needed to assess the stability of the observed separation. The fixed order of the experimental blocks is another important limitation of the design. Because MINDWANDERING, INTERNAL, and EXTERNAL were always performed in the same sequence, condition effects cannot be fully separated from possible order-related effects such as transition between tasks, adaptation, fatigue, or time-on-task. This is particularly relevant when interpreting differences between the earliest, middle, and latest INTERNAL windows. The labels correspond to instructed experimental conditions and were not independently verified during each interval. The results should therefore be interpreted as classification of instructed states rather than direct recognition of naturally occurring mind wandering or concentration.

V. CONCLUSION

The results demonstrate that the three instructed experimental conditions can be differentiated from EEG-derived features, although the degree of separability depends on both the compared conditions and the representation of the EEG data.

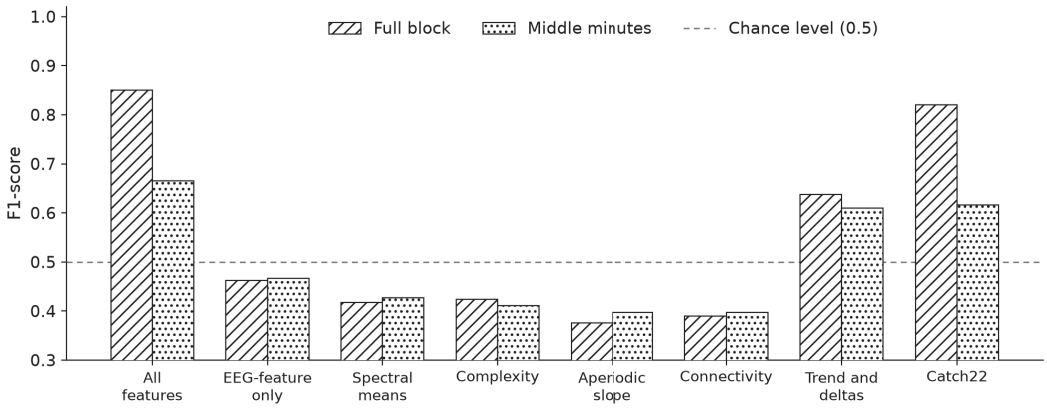


Fig. 6. MINDWANDERING–INTERNAL macro-F1 by feature family. EEG-feature only is the 22 means.

For MINDWANDERING and INTERNAL, greater separation was obtained when temporal summaries were calculated over equal-length sequences than when classification was based on a single 60-s interval or on the EEG-feature only representation. Among the matched INTERNAL windows, the middle minutes produced the highest macro-F1 of 0.665 ± 0.052.

The contrasts involving EXTERNAL were more readily separable, although this distinction also reflects differences in eye state, visual stimulation, and task demands. The findings therefore support the use of recording-level temporal information for distinguishing sustained instructed attention states, while reliable separation of MINDWANDERING and INTERNAL from individual 60-s intervals remains limited.

Further studies with larger samples, equal condition durations, counterbalanced task order, and independent verification of attention states are needed to determine the generalizability of the observed differences.

ACKNOWLEDGMENT

This work was supported by the Russian Science Foundation, project No. 25-21-00398, https://rscf.ru/project/25-21-00398/.

REFERENCES

[1] J. W. Y. Kam, T. Rahnuma, Y. E. Park, and C. M. Hart, "Electrophysiological markers of mind wandering: A systematic review," *NeuroImage*, vol. 258, p. 119372, 2022.

[2] J. W. Y. Kam, S. Rai, S. Nanjappan Jothiraj, and J. A. Helfrich, "Aperiodic and oscillatory neural activity underlying external and internal attention," *Biological Psychology*, vol. 209, p. 109307, 2026.

[3] S. Tang and Z. Li, "EEG complexity measures for detecting mind wandering during video-based learning," *Scientific Reports*, vol. 14, p. 8209, 2024.

[4] Y. Lu and J. Rodriguez-Larios, "Nonlinear EEG signatures of mind wandering during breath focus meditation," *Current Research in Neurobiology*, vol. 3, p. 100056, 2022.

[5] K. Cnudde, G. Kim, W. S. Murch, T. C. Handy, A. B. Protzner, and J. W. Y. Kam, "EEG complexity during mind wandering: A multiscale entropy investigation," *Neuropsychologia*, vol. 180, p. 108480, 2023.

[6] Y.-T. Chen, H.-H. Lee, C.-Y. Shih, Z.-L. Chen, W.-K. Beh, S.-L. Yeh, and A.-Y. Wu, "An effective entropy-assisted mind-wandering detection system using EEG signals of MM-SART database," *IEEE Journal of Biomedical and Health Informatics*, vol. 26, no. 8, pp. 3649–3660, 2022.

[7] P. Krukow, V. Rodríguez-González, N. Kopiś-Posiej, C. Gómez, and J. Poza, "Tracking EEG network dynamics through transitions between eyes-closed, eyes-open, and task states," *Scientific Reports*, vol. 14, p. 17442, 2024.

[8] Z. J. Lau, T. Pham, S. H. A. Chen, and D. Makowski, "Brain entropy, fractal dimensions and predictability: A review of complexity measures for EEG in healthy and neuropsychiatric populations," *European Journal of Neuroscience*, vol. 56, no. 7, pp. 5047–5069, 2022.

[9] T. Donoghue, M. Haller, E. J. Peterson, P. Varma, P. Sebastian, R. Gao, T. Noto, A. H. Lara, J. D. Wallis, R. T. Knight, A. Shestyuk, and B. Voytek, "Parameterizing neural power spectra into periodic and aperiodic components," *Nature Neuroscience*, vol. 23, pp. 1655–1665, 2020.

[10] H. W. Dong, C. Mills, R. T. Knight, and J. W. Y. Kam, "Detection of mind wandering using EEG: Within and across individuals," *PLOS ONE*, vol. 16, no. 5, p. e0251490, 2021.

[11] C. Y. Jin, J. P. Borst, and M. K. van Vugt, "Decoding study-independent mind-wandering from EEG using convolutional neural networks," *Journal of Neural Engineering*, vol. 20, no. 2, p. 026024, 2023.

[12] P. Kaushik, A. Moye, M. van Vugt, and P. P. Roy, "Decoding the cognitive states of attention and distraction in a real-life setting using EEG," *Scientific Reports*, vol. 12, p. 20649, 2022.

[13] A. Kashevnik, E. Glekler, E. Artemenko, I. Brak, I. Shoshina, and V. Romaniuk, "Multimodal EEG, ECG, and video dataset of yoga practitioners during concentration and mind-wandering tasks," *Scientific Data*, vol. 13, p. 850, 2026.

[14] P. D. Welch, "The use of fast Fourier transform for the estimation of power spectra: A method based on time averaging over short, modified periodograms," *IEEE Transactions on Audio and Electroacoustics*, vol. 15, no. 2, pp. 70–73, 1967.

[15] T. Higuchi, "Approach to an irregular time series on the basis of the fractal theory," *Physica D: Nonlinear Phenomena*, vol. 31, no. 2, pp. 277–283, 1988.

[16] A. Lempel and J. Ziv, "On the complexity of finite sequences," *IEEE Transactions on Information Theory*, vol. 22, no. 1, pp. 75–81, 1976.

[17] M. Vinck, R. Oostenveld, M. van Wingerden, F. Battaglia, and C. M. A. Pennartz, "An improved index of phase-synchronization for electrophysiological data in the presence of volume-conduction, noise and sample-size bias," *NeuroImage*, vol. 55, no. 4, pp. 1548–1565, 2011.

[18] C. H. Lubba, S. S. Sethi, P. Knaute, S. R. Schultz, B. D. Fulcher, and N. S. Jones, "catch22: CAnonical Time-series CHaracteristics," *Data Mining and Knowledge Discovery*, vol. 33, pp. 1821–1852, 2019.

[19] V. J. Lawhern, A. J. Solon, N. R. Waytowich, S. M. Gordon, C. P. Hung, and B. J. Lance, "EEGNet: A compact convolutional neural network for EEG-based brain–computer interfaces," *Journal of Neural Engineering*, vol. 15, no. 5, p. 056013, 2018.